Cyclic load behavior of helical pile-to-pile cap connections subjected to uplift loads

Serhan Guner [*], Sundar Chiluwal

Department of Civil and Environmental Engineering, University of Toledo, Toledo, OH 43607, USA

ARTICLE INFO

ABSTRACT

Although significant research has been conducted on helical piles, there is a lack of research and official design guidelines on how to create resilient helical pile-to-pile cap connections, especially in tall and light structures where tensile uplift loads may govern the foundation design. The objective of this study is to advance the current understanding, quantify the influence of helical pile-to-pile cap connection detailing on the global system behavior, and propose recommendations for their resilient design. For this purpose, high-fidelity nonlinear finite element models are developed, experimentally verified, and 162 response simulations of helical pile cap systems are conducted to quantify the influences of: termination bracket types, bracket embedment depths, reinforcement ratios, shear span-to-depth ratios, and loading types. The results are analyzed in terms of the load, deformation, cracking, and failure behaviors. The analysis of variance and the factorial design methods are employed to quantify the percentage contribution of each parameter, as well as multi-parameter interactions, on the system capacity. The results, which are also applicable to micropile connections, demonstrate that the helical pile-to-pile cap connection capacity may govern the system capacity for the load conditions involving tension components. The tension load capacities of the pile cap systems (all of which are doubly and symmetrically reinforced) are found to be only 54% of their compression load capacities due to connection zone failures. This result is in contrast with the results from the traditional sectional analysis methods, which are not intended for the analysis of the connection zones and thus calculate the tension and compression capacities as equal. This paper presents the studies undertaken, conclusions reached, and recommendations made to create resilient helical pile-to-pile cap connections.

1. Introduction

Many structures are subjected to cyclic loads that promote the sequential application of compression and tension loads due to events such as windstorms, earthquakes, or heavy vehicular traffic. Tall and light structures – such as telecommunication or transmission towers, wind turbines, and light-frame steel buildings – are particularly vulnerable to the tensile uplift loads due to large overturning moments (e.g., Fig. 1). These forces must be safely resisted by the foundations during the entire service life without cracking, settlement, or excessive deformations.

Helical piles (see Fig. 2a) inherently possess high resistance to uplift forces, thereby presenting a significant potential to create resilient, durable, and faster-to-construct foundations. Helical piles are commonly connected to the superstructures through concrete foundation elements, such as pile caps, mat or strip footings, and grade beams, where they are

terminated with a steel plate or bracket. The common bracket types used in today's construction practice include the single-plate (see Fig. 2a and 2b) and, less commonly, double-plate and studded-plate types (see Fig. 2c and 2d). These connections, including the surrounding concrete (termed as the connection zone), should be able to resist major cyclic load demands while remaining crack-free and rigid.

Despite the critical importance of helical pile-to-pile cap connections, there is a lack of research, understanding, and official design guidelines on how to analyze and design these connections to resist the uplift load demands. The helical pile research is typically conducted by geotechnical specialists while the concrete foundation research is conducted by structural specialists. The geotechnical literature primarily focuses on the axial load behavior of isolated or group piles and consistently demonstrates the suitability of helical piles for the load cases including tensile uplift [3-10] and compression [8,11-17]. The structural literature, on the other end, focuses on the behavior of
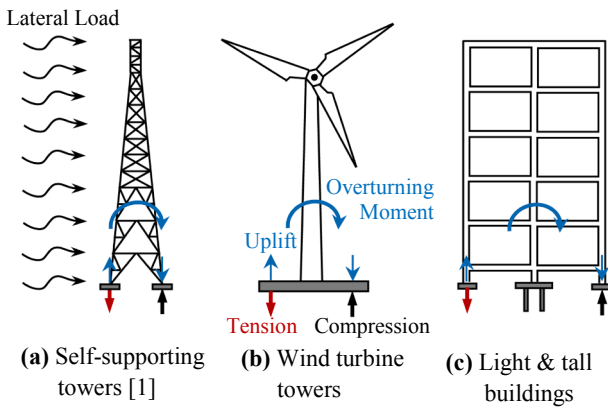

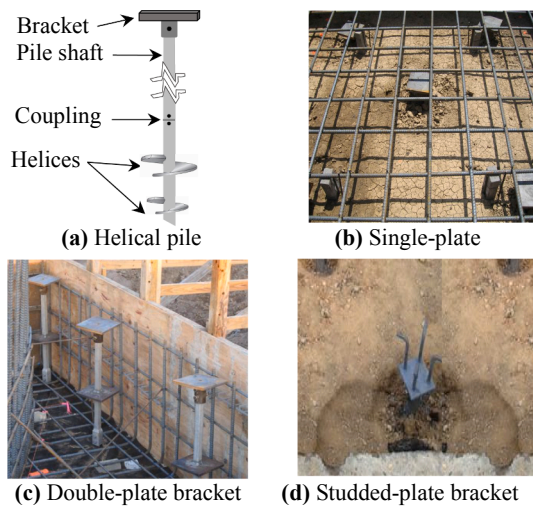**Fig. 1.** Sample structures subjected to tensile uplift loads.

Fig. 2. Helical pile termination bracket types [2].

traditional concrete pile caps supported by socketed concrete piles, subjected to compression and shear loads [18-38]. The connection research is left at the intersection without receiving full attention.

There is neither a clear understanding nor proven analysis methods for creating reliable and efficient helical pile-to-pile cap connections for tension load resistance. These connections are commonly designed in practice using 'rules of thumb' or code expressions, such as punching shear checks, which are not intended for this purpose. An experimental study conducted by Diab [39] demonstrates that the connection behavior might govern the entire system response. Another study [40] investigated the failure of an Olympic-size swimming pool supported by helical piles and found that the pool collapsed due to the connection failure under uplift water pressure. In addition, the connection design should prevent potential concrete cracks under daily service loads to ensure long-term durability without water penetration, steel corrosion, concrete spalling, and excessive deformations. These examples highlight the importance of understanding and explicitly accounting for the connection response when designing helical foundation systems.

The objective of this study is to advance the current understanding, quantify the influences of helical pile-to-pile cap connection detailing on the global system behavior, and propose recommendations for their resilient design subjected to cyclic load reversals with tension components. Using state-of-the-art high-fidelity nonlinear analysis methods, numerical models are developed, experimentally verified, and 162 simulations are performed to understand and quantify the influences of the bracket types, bracket embedment depths (h_e), pile cap longitudinal reinforcement ratios (ρ_x) and shear span-to-depth (a/d) ratios, and the

loading conditions. Additionally, the contributions and interactions among these variables are examined using the analysis of variance (ANOVA) and factorial design approaches. The design configurations that result in premature concrete cracking or undesirable responses are identified. The numerical results, which inherently include the influence and failure modes of the helical pile-to-pile cap connections, are compared with the traditional global analysis methods (i.e., sectional flexure and shear) to assess the significance of considering or neglecting the connection response when designing helical foundation systems. While the failure modes associated with soil is outside the scope of this study, the readers are referred to the references cited above for such studies and Ref. [41] for a system-level modeling methodology.

2. Foundation system details

An archetype concrete foundation strip, representative of a commonly used pile cap configuration, was designed following the CRSI [42] and Guner and Carrière [1] recommendations. The strip is supported by two helical piles to create a one-way stress flow and better isolate the connection response. The helical piles are terminated with one of the three bracket types: single bracket (see Fig. 3a), double bracket (see Fig. 3b), and studded bracket (see Fig. 3c). All bracket plates have the same dimensions and material properties to facilitate a consistent comparison. Influencing parameters investigated include: three h_e for the single bracket [i.e., 460 mm (top), 300 mm (middle), 140 mm (bottom)]; one h_e for the double bracket [i.e., 460 mm]; two h_e for the studded bracket [i.e., 300 mm (middle), 140 mm (bottom)]; three ρ_x for all bracket types [i.e., minimum 0.2% (5-#5 rebars) from ACI 318–19 [43], 0.4% (7-#6 rebars), and 0.8% (10-#7 rebars)]; and three a/d ratios for all bracket types [i.e., 1.68, 1.42, and 1.11]. When considering the three loading conditions (i.e., monotonic tension, monotonic compression, and reversed cyclic), 162 design configurations are created [$(3 + 1 + 2) \times 3 \times 3 \times 3 = 162$].

3. Nonlinear finite element modeling approach

A two-dimensional (2D), continuum-type, and plane-stress element is used for the finite element modeling of the pile cap through the computer program VecTor2 [44]. The formulation is based on the Disturbed Stress Field Model [45], which is an extension of the Modified Compression Field Theory (MCFT) [46] – a theory adopted by several design standards [e.g.,47,48]. The MCFT employs a smeared, rotating crack approach within a total-load, secant-stiffness solution algorithm, and allows the consideration of the coupled flexure, axial, and shear effects in a concrete element. The MCFT uses the average and local strains and stresses in the concrete and reinforcement, and the widths and orientations of cracks as the plastic deformations and damage accumulate in the post-peak region. Although a 2D model, the triaxial concrete confinement is accounted for by in- and out-of-plane reinforcement components. Additionally, VecTor2 incorporates a number of advanced material behavior models that are specific to reinforced concrete, some of which are listed in Table 1. Important in this study, the reversed-cyclic concrete and steel material hysteresis models, and the load application protocols are shown in Fig. 4, where f_c and f_s are the concrete and steel stresses, ε_c and ε_s are the concrete and steel strains, and E_s is the elastic modulus of the steel. More information on these models is provided elsewhere [49].

3.1. The equivalent cone method (ECM)

Two-dimensional (2D) numerical models are computationally more efficient and faster than the 3D models. One limitation of 2D models is the assumption that stresses and strains are constant through the thickness of the member. In reality, however, the stresses tend to propagate in a conical shape from the tips of the termination plate towards the surface of the concrete. When the tension capacity of the
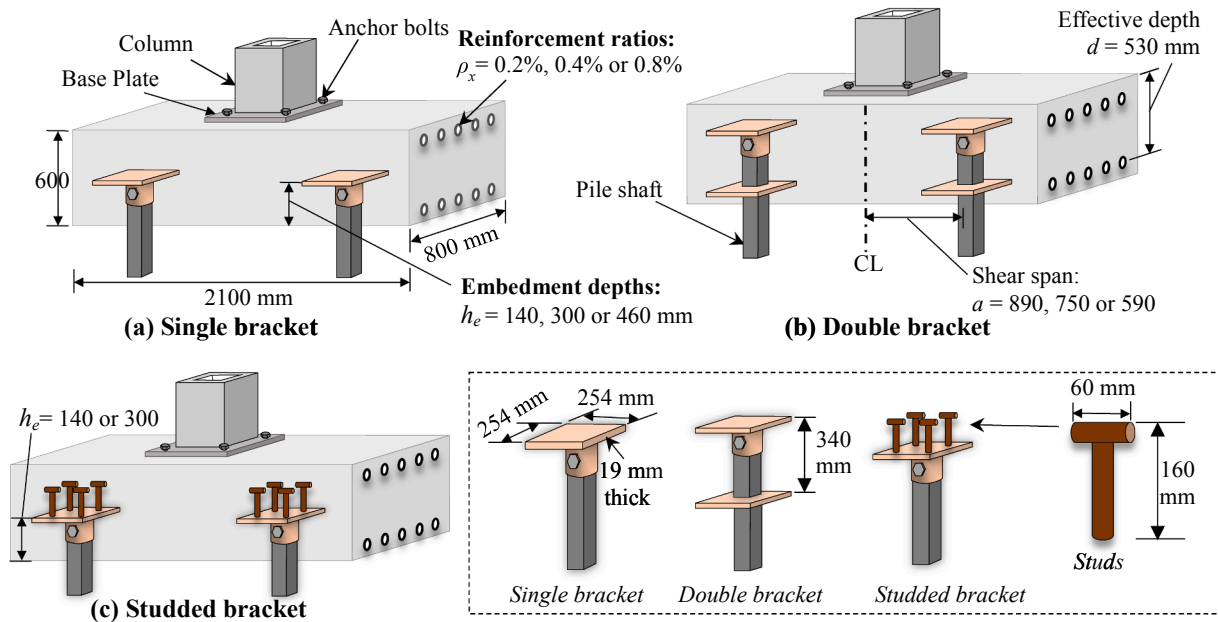
Fig. 3. Foundation and connection configurations examined.

Table 1
Material constitutive models used.

| Material Behaviour	Default Model
Concrete	
Compressive Base Curve	Hognestad
Compression Post-Peak	Modified Park-Kent
Compression Softening	Vecchio 1992
Tension Stiffening	Modified Bentz 2003
Tension Softening	Linear
Confined Strength	Kupfer/Richart
Concrete Dilation	Variable-Isotropic
Cracking criterion	Mohr-Coulomb (Stress)
Crack Width Check	Agg/5 Max crack width
Crack Slip	Walraven
Reinforcing Bars	
Hysteretic Response	Seckin w/ Bauchinger
Dowel Action	Tassios (Crack Slip)
Buckling	Akkaya et al. 2019 [50]
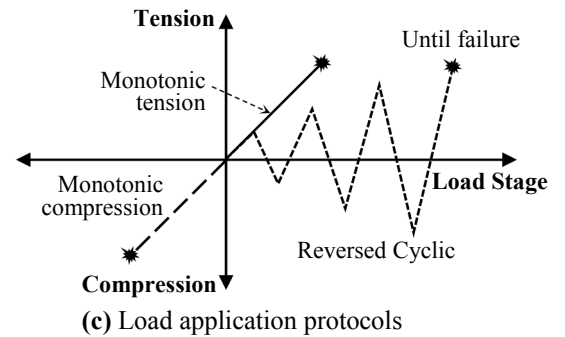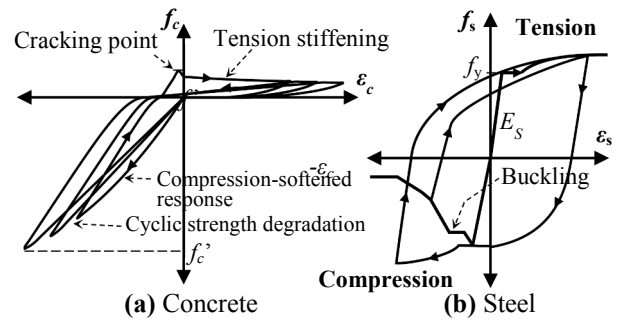
Fig. 4. Material hysteresis models and loading protocols used.

concrete governs, a concrete breakout or cone failure occurs (to be demonstrated in Fig. 11), resulting in a conical cracking pattern that cannot be naturally captured by 2D NLFE models. To overcome this limitation, the Equivalent Cone Method (ECM) [51] is employed. This method determines an equivalent concrete thickness (t_{2D}) for use in 2D models to a yield breakout failure load that is approximately equal to the load which would be predicted by a 3D model employing the same theoretical basis (see Fig. 5). The steps and equations of this method can be found elsewhere [51-54].

3.2. Numerical models

One sample numerical model developed for each bracket type is presented in Fig. 6, where the concrete is modeled using four-node rectangular elements with eight degrees of freedom each, and the longitudinal reinforcement is modeled using two-node discrete truss bar elements with four degrees of freedom each. A fine mesh with a size of 20 mm × 20 mm was used and each helical pile is restrained with four hinges to better isolate the pile cap response. A displacement-controlled analysis was employed, which is advantageous when simulating the post-peak response, ductility, crack patterns, and failure modes. The loading was applied at the topmost ends of the anchor bolts with small
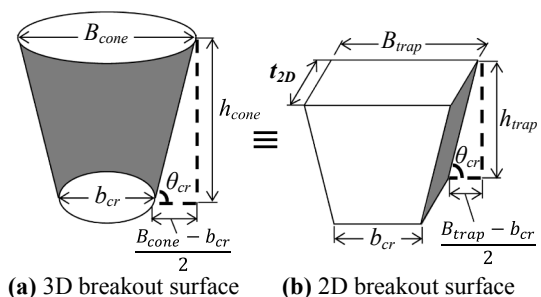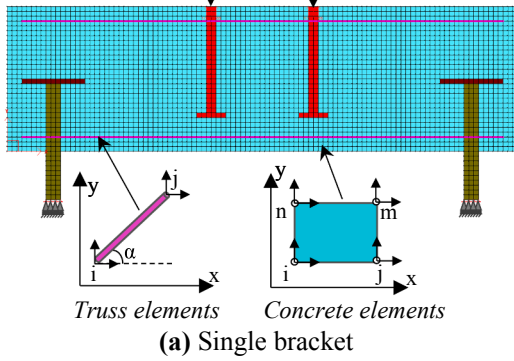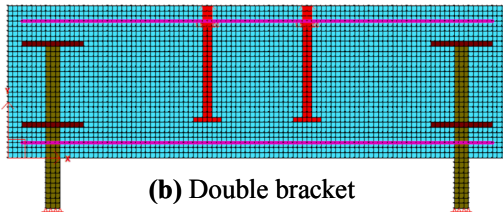

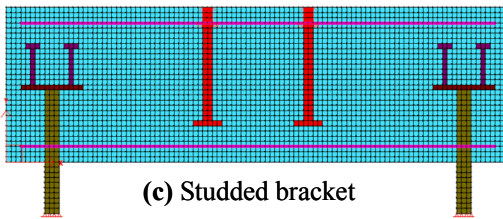**Fig. 5.** Modeling concrete breakout failure using 2D models [51].

Loading: Tension, Compression, or reversed-cyclic

Truss elements   *Concrete elements*

(a) Single bracket

(b) Double bracket

(c) Studded bracket

Refer to Fig. 3 for detailed model dimensions.

Fig. 6. Samples of numerical models developed.

Table 3
Truss bar properties.

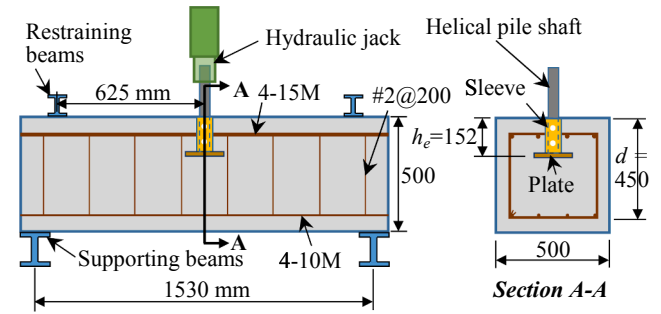| Truss	Description	Color	f_y (MPa)	ρ_x
1	Longitudinal bars		414	0.2%, 0.4%, or 0.8%

Fig. 7. Experimental test setup for Specimen T1 [39].

Table 4
Test specimen dimensions [39].

Specimen	f'_c (MPa)	h_e (mm)	b_w (mm)	ρ_x	ρ_y (#2@200)
T1	30	152	165	4–15 M	2 legs
T2	30	203	165	4–15 M	2 legs
T3	30	254	165	4–15 M	2 legs
T4	40	203	190	4–15 M	2 legs
T5	40	203	229	4–15 M	2 legs
T6	40	203	165	4–20 M	2 legs
T7	40	203	165	4–25 M	2 legs
T8	40	203	165	4–15 M	4 legs
T9	40	203	165	4–15 M	2 legs

Bar areas: 15 M = 200, 20 M = 300, 25 M = 500, #2 = 32 mm^2

Fig. 8. Numerical model for Specimen T4.

displacement increments in the range of 0.20 to 0.25 mm. An average equivalent concrete thickness of 800 mm is used for all numerical models to allow for a consistent comparison. Tables 2 and 3 show the component properties in terms of their strengths and dimensions.

3.3. Verification of the modeling approach

To verify the numerical models developed in this study, the results from an experimental study involving similar specimen and loading conditions were used. The experimental study tested nine specimens consisting of a single bracket embedded into 500 × 500 × 1600 mm pile cap specimens shown in Fig. 7. Note that the test setup is an inverted pile cap. The parameters investigated were termination plate embedment depth h_e, longitudinal reinforcement ratio ρ_x, bracket width b_w, shear reinforcement ratio ρ_y, and the concrete compressive strength f'_c. The configurations tested are presented in Table 4; more details can be found elsewhere [39].

Only one half of the pile caps are modeled (see Fig. 8) to reduce the computational cost, taking advantage of the symmetry. A horizontal roller is used at the top of the steel support plate while vertical rollers are
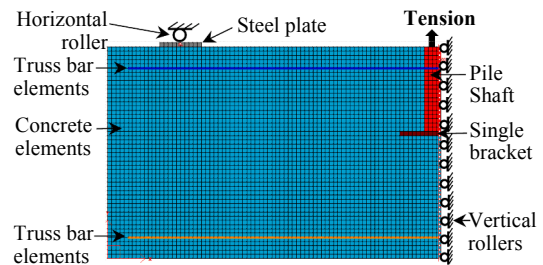
added to the right edge to account for the symmetry. The load is applied as an uplift displacement at the top of the bracket in small displacement steps. Using the ECM [51], the equivalent thickness of the specimens for use in the 2D models are calculated to range between 327 mm and 417 mm. More details can be found elsewhere [55].

The load capacities obtained from the numerical simulations are compared to the experimental ones as shown in Fig. 9. Comparison results indicate that the simulations captured the experimental results with an excellent accuracy –simulated-to-experimental ratio average of 1.01 with a coefficient of variation 6%.

Two sample load–displacement response simulations are presented in Fig. 10. The numerical simulations are in good agreement with the experimental results, able to accurately simulate the nonlinear stages of the overall behavior. The initial stiffnesses, which are not the focus of this study, are somewhat overestimated. This phenomenon is commonly encountered in numerical simulations due to various effects such as: the perfect supports used in the simulations versus the experimental supports and loading system which may exhibit some flexibility, and
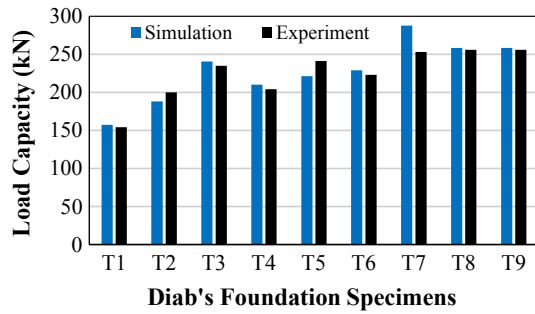
Table 2
Continuum region properties.

Region	Description	Color	f'_c (MPa)	f_y(MPa)	Thickness(mm)
1	Concrete		20.7	–	800
2	Helical Piles			552	44
3	Bracket Plates		–	345	260
5	Anchor Bolts		–	724	57
6	Studs		–	420	14

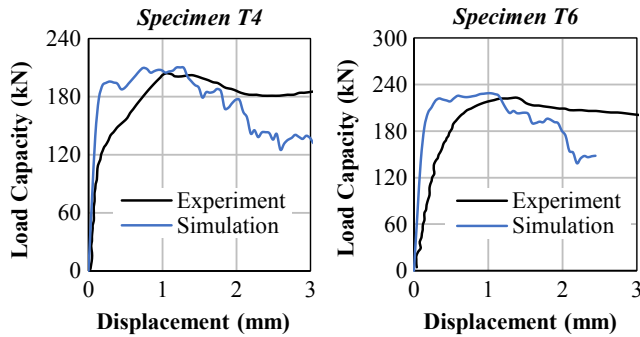**Fig. 9.** Verification of the numerical modeling approach.

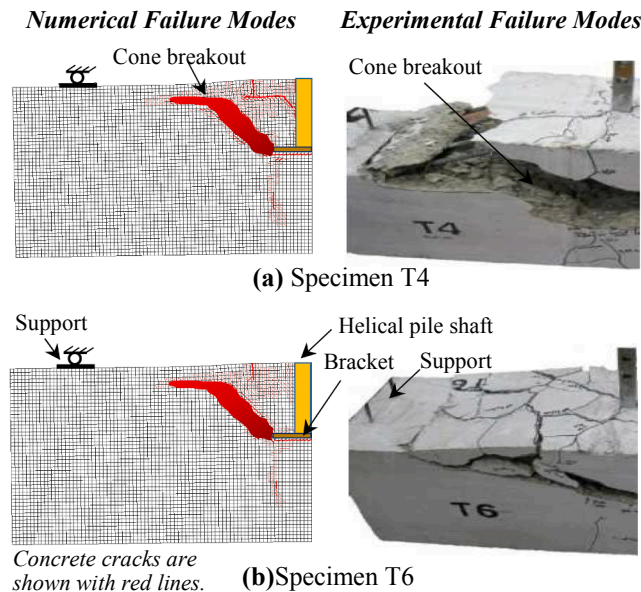**Fig. 10.** Verification of load–displacement responses.

Fig. 11. Verification of crack patterns and failure modes.

potential shrinkage cracks in the experimental specimens versus perfectly uncracked and unstressed numerical models. The failure modes and crack patterns are also simulated very well (see Fig. 11).

4. Simulation results

The results from the 162 numerical simulations were systematically analyzed and compared according to the loading cases to which they are subjected. The reversed-cyclic-load results are divided into two parts and investigated as cyclic tension and cyclic compression (see Fig. 12a). These two load cases are compared with the monotonic tension and

monotonic compression load cases (see Fig. 12b and 12c). The load capacity is defined as the peak load that can be resisted by the pile cap configuration.

4.1. Tension behavior (Monotonic and cyclic tension cases)

The simulation results are analyzed in terms of the peak load capacities, h_e, a/d ratios, and ρ_x ratios. The results are graphically presented in Fig. 14a, 14b, and 14c, each of which contains 27, 9, and 18 simulation results, respectively. The results demonstrate that the load capacity increases by an average of 30% when the h_e is changed from bottom to middle. This capacity gain can be explained by the increase in the concrete mass in front of the helical pile bracket which yields a larger tensile failure surface. In agreement with this finding, a connection zone failure mode is predicted for the bottom h_e (to be discussed in Section 5). The further increase in h_e from middle to top does not affect the capacity, as shown by the overlapping of the red and green lines in Fig. 13a. When inspecting the failure modes, it becomes clear that both models (with middle and top h_e) fail with a global failure mode and that the connection zone failure does not govern the system response. The double bracket has only one h_e position, which exhibits a good performance such that the connection zone conditions do not govern the system capacity (see Fig. 13b). The studded bracket has two h_e positions, and the change in h_e does not influence the load capacity (see overlapping lines in Fig. 13c) except for the higher ρ_x ratios where the increased system load capacity results in connection zone cracking in the bottom h_e position such that connection zone starts to influence the response (see the deviation in the dashed and dotted lines in Fig. 13c). If the bottom h_e must be used, the change of the bracket type from single to studded improves the system capacity by an average of 29% for monotonic tension (compare the slopes and positions of blue lines in Fig. 13a and 13c). The a/d ratio, which signifies how deep a concrete member is, affects the system capacity significantly with lower ratios (i.e., deeper members) providing exponentially higher system capacities as indicated by the bi-linear nature of the lines in Fig. 13a to 13c. The cyclic tension load case results (as presented in Fig. 13d, 13e, and 13f) confirm the same findings with slightly smaller load capacities as expected due to cyclic damage. In both loading conditions, the tension capacity of all bracket types increases significantly with higher ρ_x with the exception of the bottom h_e where the connections zone failure prevents any significant capacity increase with higher ρ_x.

4.2. Compression behavior (Monotonic and cyclic compression cases)

The simulation results are analyzed, using the same methodology as in Section 4.1, and presented graphically in Fig. 14. The overlapping nature of the lines of different colors demonstrates that the compressive load resistance is independent of the changes in h_e for all the bracket types. This can be explained by the absence of connection zone cracking or failure under compressive loading. One exception is the top h_e of the single bracket in higher ρ_x configurations, subjected to reversed-cyclic loads (see the dotted lines in Fig. 14d for deviations and in Fig. 14e for the reduced rate of capacity increase). Due to the cyclic damage in the tensile direction of the loading, the connection zone exhibits cracking, thereby reducing the compression load capacities in these configurations. In all configurations, the load capacity increases with the increase in ρ_x and decreases in a/d ratios, similar to those in the tension loading.

4.3. Tensile versus compressive load capacities

Fig. 15 presents the average load capacities obtained from the 54 simulations of all connection types in a particular loading type, including the monotonic tension, monotonic compression, and reversed-cyclic cases ($54 \times 3 = 162$ simulations in total). The results indicate that the average system failure load in tension is merely 54% of that in the
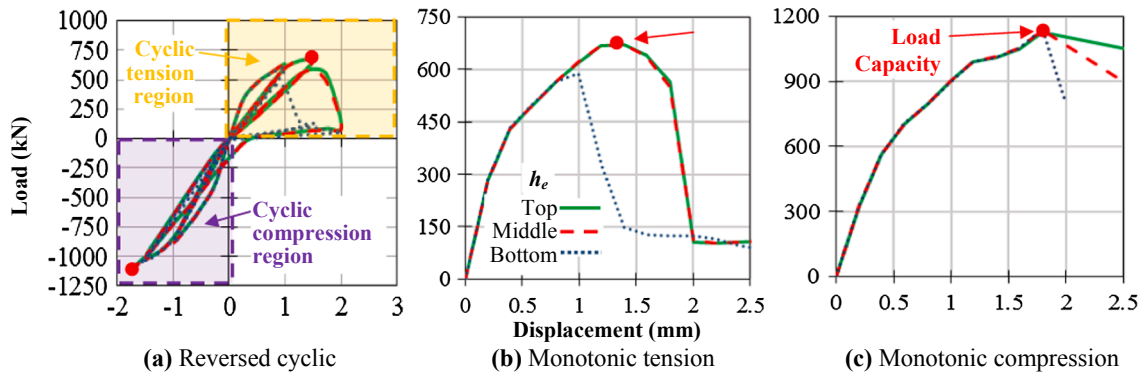
Fig. 12. Naming convention for load cases and the load capacity points (sample results shown for the single bracket).
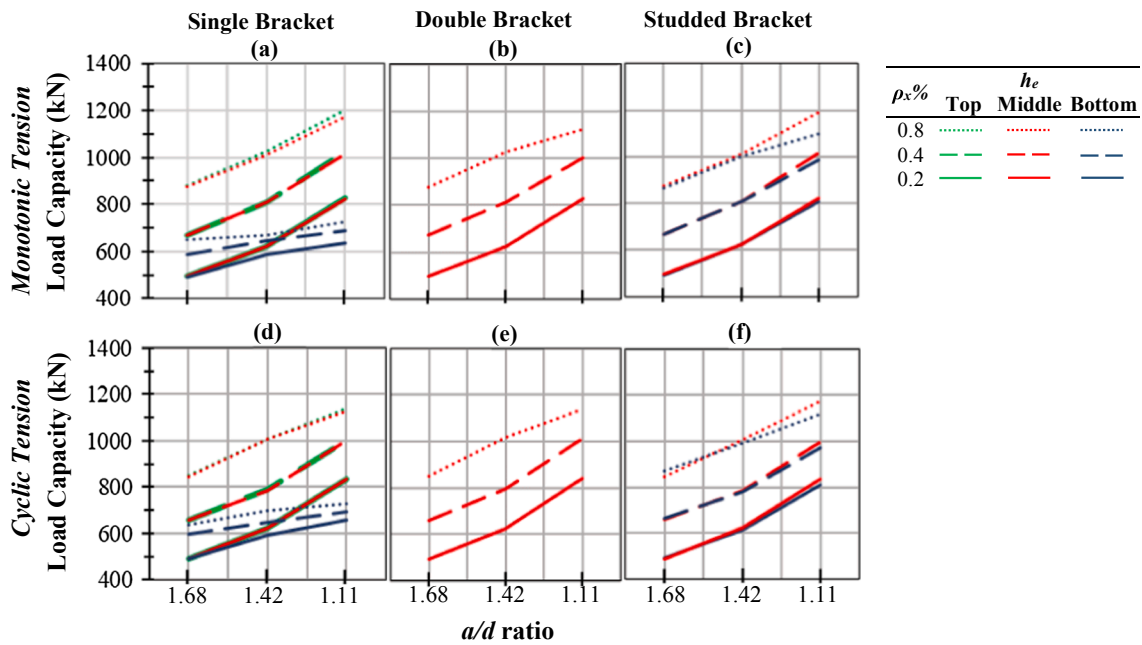

Fig. 13. Load capacities at system failures subjected to tension loads.

compression load. This result agrees well with Diab's experimental results [39] where this value is 55%. It should be noted that a small number of load cycles were applied in this study to keep the computational demand at reasonable limits. It is expected, in reality, that the cyclic damage and the load capacity degradation would be higher due to a larger number of load cycles from wind and other lateral loads during the lifetime of light and tall structures. It is of interest to note that the pile caps examined in this study are doubly and symmetrically reinforced, and if analyzed with the traditional sectional analysis methods (to be discussed in Section 7), their load capacities in tension (i.e., the point load applied upwards) and compression (i.e., the point load applied downwards) would be calculated as equal.

5. Crack patterns and failure modes

The simulated deflected shapes, crack patterns, and failure modes are presented in Fig. 16 for the selected, representative specimens. Major connection zone cracking and even failures are predicted for some of the specimens subjected to monotonic tension and reversed-cyclic loading. The bottom h_e of the single bracket type exhibited the least favorable performance of all bracket types examined in this study by sustaining connection zone failures (see Fig. 16a and 16 g). While performing better, the bottom h_e of the studded bracket type exhibited

major connection zone cracking (see Fig. 16c), which reduced the system capacity by up to 10%. This type of cracking may be detrimental to long-term durability. The middle and top h_e of the single bracket (Fig. 16b and 16 h), the middle h_e of the studded bracket (Fig. 16d), and the double plate bracket (Fig. 16e and 16f) performed satisfactorily with no major connection zone cracking. The double plate bracket type may provide additional advantages such as resilience to other types of loads and long-term durability due to its extended shaft and top and bottom plates confining the entire depth of the pile cap. Subjected to pure compression loads, all specimens with all bracket types exhibited global failure modes of flexure and shear, without exhibiting any major connection zone cracking (Fig. 16i and 16j).

6. Contributions and interactions of design parameters

To better understand and quantify the influence of the investigated parameters (i.e., bracket types, h_e, ρ_x, a/d ratios, and loading types) on the system-level load capacities, two statistical analysis methods were employed: the analysis of variance (ANOVA) and factorial design [56]. These methods are particularly useful to assess if the changes in the simulation result due to the changes in single or multiple parameters are statistically significant or not [57]. The analysis of variance relies on partitioning the total variability of the collected dataset into its
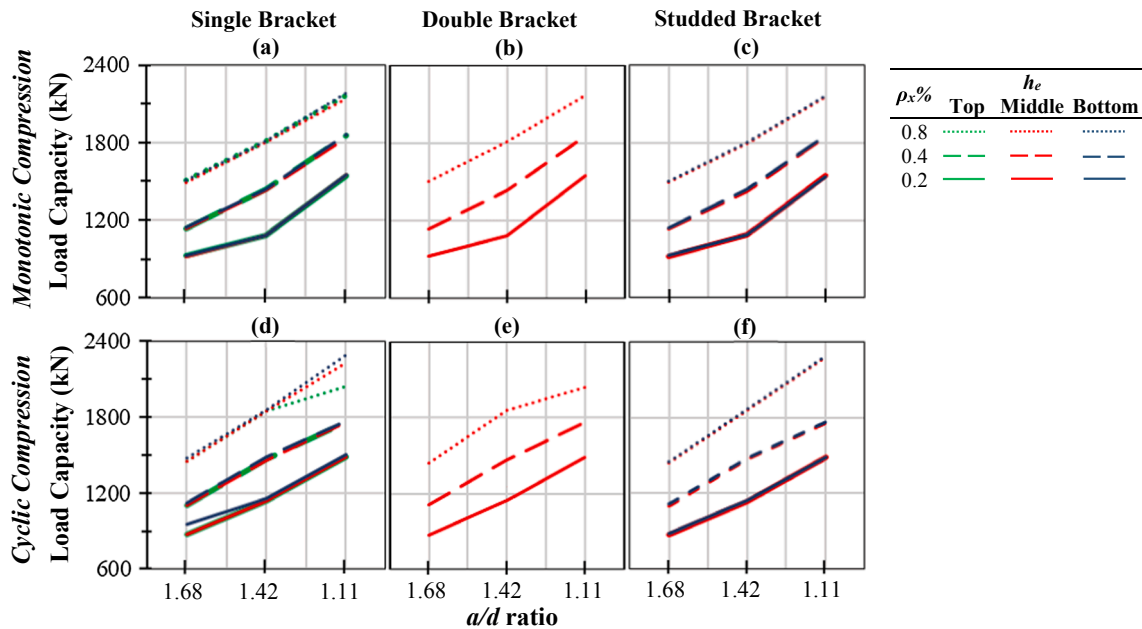
Fig. 14. Load capacities at system failures subjected to compression loading.
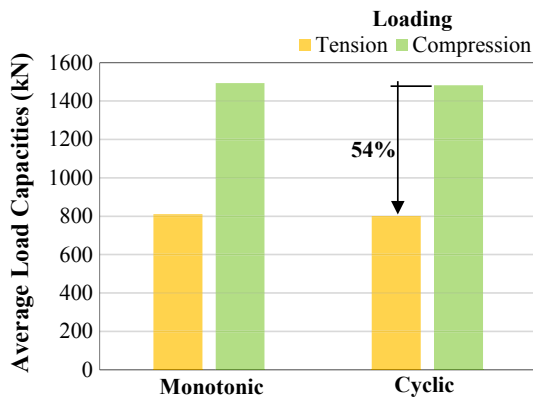

Fig. 15. Average load capacities of all simulations.

components. The total sum of squares is used as a measure of the overall variability in the data. The results are analyzed under percentage contributions, which is the measure of the contribution of each parameter's effect (and their respective interactions in the case of multiple parameters) relative to the total sum of squares.

Table 5 shows the contributions of each parameter to the system-level peak load capacities for the single bracket type. The results for the tension load case indicate that the a/d ratio, ρ_x, and h_e parameters dominate the response, accounting for 87.8% of the total variability, whereas two- and three-parameter interactions account for the remaining 12.2%. This conclusion diverges from the compression load case, where parameter h_e, and two- and three-parameter interactions are found insignificant. Both results are also confirmed with the ANOVA method. More details on these calculations can be found elsewhere [55].

The a/d ratio-ρ_x, a/d ratio-h_e, and ρ_x-h_e, interactions are plotted in Fig. 17. The similar slopes of the curves in Fig. 17a verifies the conclusion of no interaction between a/d ratio-ρ_x parameters, while the different slopes in Fig. 17b and 17c show interactions between ρ_x - h_e and a/d ratio-h_e parameters. Fig. 17b and 17c show that there is no difference in the tension load capacity when the middle or top h_e is used while the bottom h_e provides significantly smaller capacities. The discrepancy in the load capacity between the bottom h_e and the other two h_e

increases as ρ_x increases or a/d ratio decreases (i.e., the pile cap becomes thicker). The combined analysis of Fig. 17 can be used to conclude that the combination of low a/d ratio, high ρ_x, and either mid or top h_e yields the highest tension load capacity.

7. Comparisons with traditional sectional analysis methods

Both the numerical simulations (performed in this study) and the experimental tests (performed in reference [39]) inherently include the influence and failure modes of connection zones. The traditional sectional analysis methods, on the other hand, consider the concrete pile cap globally while neglecting the local influences such as how the load is introduced or how the supports and connection zones are detailed. This approach is intended for traditional design cases where the local influences introduce compression to the member, thereby locally increasing the connection capacity. If these local influences, however, introduce tension, the connection capacity could be lower than the member capacity and a separate connection capacity assessment would be required as per, for example, ACI 318–19 [43] clause 9.4.3.2 or CSA A23.3–14 [47] clause 11.3.2.1. To assess the significance of considering or neglecting the connection capacity under tension loads, the experimental specimens are analyzed with the sectional methods contained in the ACI 318–19 standard [43]. The sectional method requires the calculation of the shear and flexural capacities at the most critical sections and comparing them with the shear and moment demands.

It is clear from Fig. 18 that the experimental capacities are much smaller than those predicted by the sectional analysis method. This result confirms that the connection capacity governs the entire system response of these specimens and that the use of the sectional analysis overestimates the system capacity by a factor of 2.2 on average.

8. Conclusions and recommendations

The influence of helical pile-to-pile cap connection detailing on the global load, deformation, cracking, and failure behaviors of concrete pile cap systems are studied. The parameters investigated are summarized in Fig. 19.

The results of the investigations demonstrate that the helical pile-to-pile cap connection capacity may govern the system capacity for the load conditions involving tension components. The traditional global
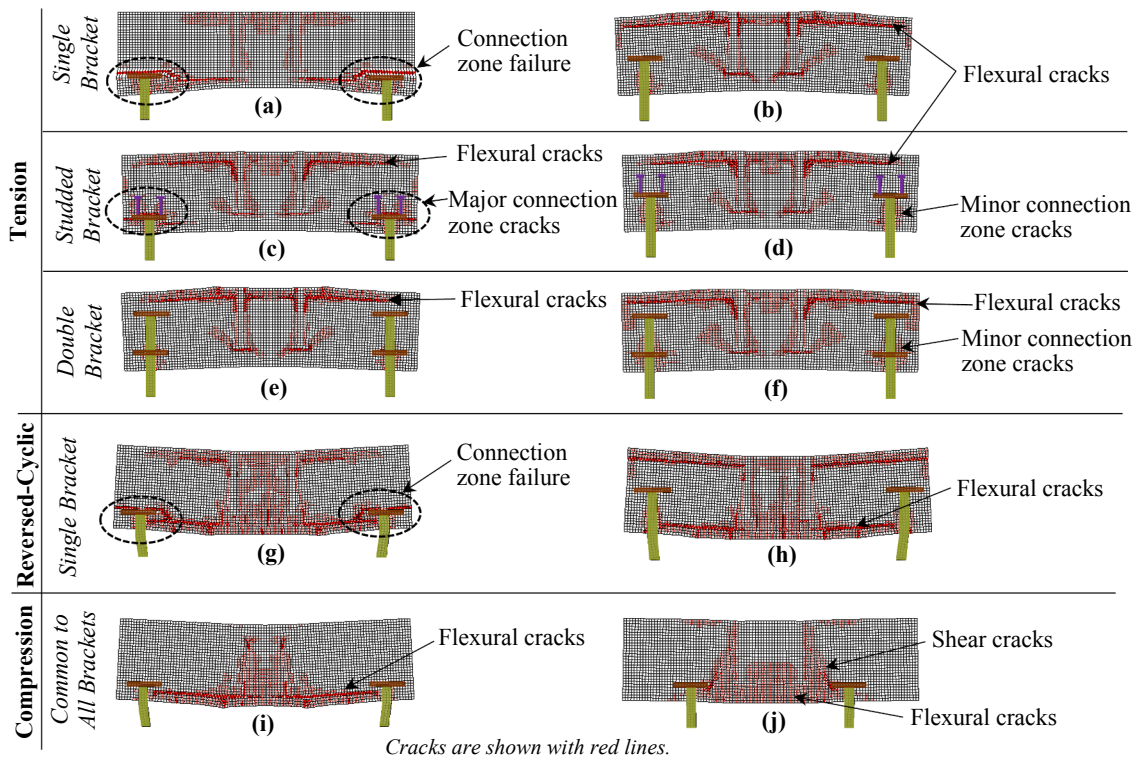
Fig. 16. Representative failure modes and crack patterns for the pile cap configurations examined.

Table 5
Contributions of parameters to the system load capacity.

Parameters	Monotonic Tension Contribution	Monotonic Compression Contribution
ρ_x	35.8%	46.9%
a/d ratio	28.1%	52.5%
h_e	23.9%	0.0%
ρ_x-h_e	7.0%	0.0%
a/d ratio-h_e	4.9%	0.0%
a/d ratio-ρ_x-h_e	0.2%	0.0%
a/d ratio-ρ_x	0.1%	0.6%
Total	100%	100%

analysis methods, which are not intended for the analysis of the connection zones, are found to significantly overestimate the capacity of the helical pile cap systems exhibiting connection zone failures by a factor of 2.2 on average. The results justify the recommendation of performing an explicit capacity check of the connection zones in addition to the structural and geotechnical checks if one of the foundation load cases include tension or pullout loads. Detailed conclusions and recommendations are provided below.

8.1. Monotonic and cyclic tension

- The helical pile-to-pile cap connection zone detailing influences the global load capacity of the pile cap systems. When designing the helical pile-to-pile cap connections, special attention should be given to light and tall structures where one of the foundation load cases may be tensile in nature.
- The tension load capacities of the pile cap systems (all of which are doubly and symmetrically reinforced) are found to be only 54% of their compression load capacities. If analyzed with the traditional sectional analysis methods, which are not intended for the analysis of the local connection zones, their load capacities in tension and compression would be incorrectly calculated as equal.
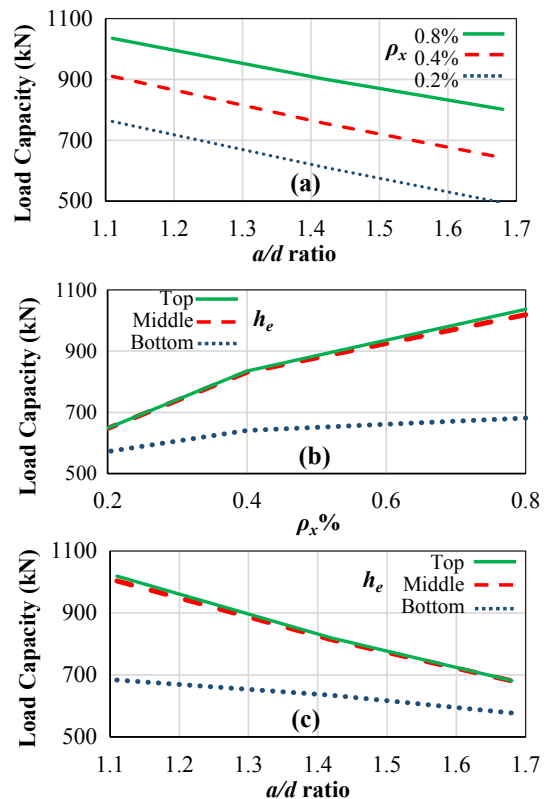

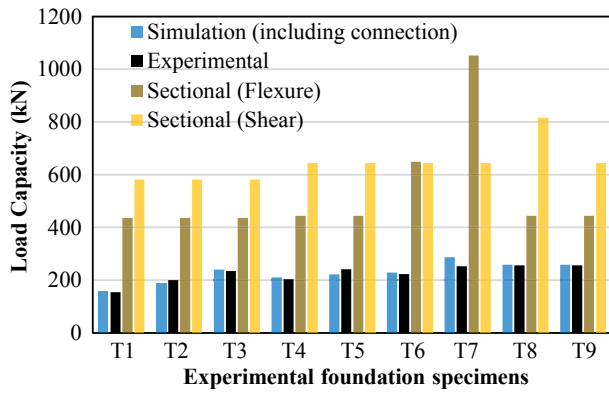Fig. 17. Interaction among parameters subjected to monotonic tension.

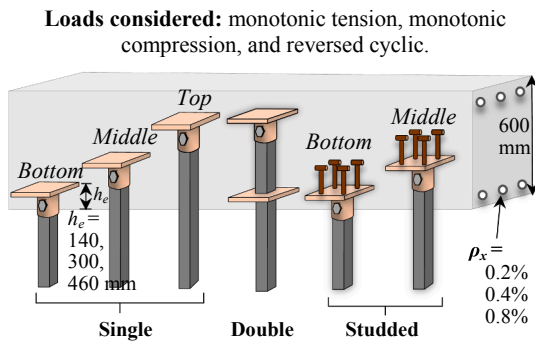**Fig. 18.** Tension load capacities calculated using various methods.

Fig. 19. Summary of the design parameters investigated.

- Connection zone failure is predicted for the bottom h_e of the single bracket type, with a decrease in the global load capacity by 25% on average. It is recommended that the middle h_e be used if the single bracket termination is to be used.
- The statistical analysis of the results indicates that the combination of low a/d ratios, high ρ_x, and the middle h_e yields the highest tension load capacity for the single bracket. These analyses also indicate that h_e dictates the effectiveness of ρ_x and a/d ratio. In other words, if larger tension load capacities are desired, h_e should be changed from bottom to middle, as opposed to using the bottom h_e and increasing the ρ_x ratio or reducing the a/d ratio with hopes to increase the global load capacity (which is not effective).
- The double bracket type has only one embedment depth which provides satisfactory responses with no connection zone failure in all simulations contained in this study.
- The studded bracket type has two h_e positions. While no connection zone failure is predicted, major connection zone cracking is observed for the bottom h_e. For the configurations involving the bottom h_e, the change of the bracket type from single to studded improves the system capacity by an average of 22%; consequently, the studded bracket may be preferred over the single bracket for the bottom h_e. For the most optimum results, however, the middle h_e is recommended for both the single and studded bracket types.
- Although the bottom h_e of the single bracket type demonstrated the least-favorable behavior, it can still be successfully used for resisting uplift forces if a special connection zone detailing is developed (e.g., sufficient amounts of vertical ties or stirrups in the connection zone). This recommendation is also applicable to the bottom h_e of the studded bracket type.

8.2. Monotonic and cyclic compression

- The helical pile-to-pile cap connections are found to not influence the monotonic compression load capacity of the helical pile cap systems in any of the bracket types examined; no connection failures are predicted.
- The statistical analyses show that the h_e parameter has no significant contribution to the monotonic compression capacity of the helical pile cap systems.
- To maximize the load capacity, high ρ_x, and low a/d ratios should be used for all bracket types.
- The compression capacity of the pile cap systems examined is found, on average, to be 1.85 times higher than their tension capacity.
- For the cyclic compression loading, connection zone cracks and reduced load capacities (up to 10%) are predicted for the top h_e of the single bracket in some design configurations. It is recommended to follow the tension load recommendations for the load cases involving cyclic load reversals.

Declaration of Competing Interest

The authors declare that they have no known competing financial interests or personal relationships that could have appeared to influence the work reported in this paper.

Appendix A. Supplementary material

Supplementary data to this article can be found online at https://doi.org/10.1016/j.engstruct.2021.112667.

References

[1] Guner S, Carrière J. Analysis and strengthening of caisson foundations for uplift loads. Can J Civil Eng 2016;43(5):411–19. Retrieved from https://www.utoledo.edu/engineering/faculty/serhan-guner/docs/JP6_Guner_Carriere_2016.pdf [accessed 07/05/2021].

[2] Supportworks 2018. Source of the figures used. Retrieved from https://commercial.supportworks.com/case-study/case-studies.html [accessed 07/05/2021].

[3] Tsuha CDHC, Filho JMSMDS, Santos TDC. Helical piles in unsaturated structured soil: a case study. Can Geotech J 2016;53(1):103–17. https://doi.org/10.1139/cgj-2015-0017.

[4] Schiavon JA. Behaviour of helical anchors subjected to cyclic loadings. PhD Dissertation. Civil Engineering. École centrale de Nantes. Universidade de São Paulo (Brésil); 2016. In English. https://10.11606/T.18.2017.tde-10072017-090437.

[5] Wang D, Merifield RS, Gaudin C. Uplift behavior of helical anchors in clay. Can Geotech J 2013;50(6):575–84. https://doi.org/10.1139/cgj-2012-0350.

[6] Merifield RS. Ultimate uplift capacity of multiplate helical type anchors in clay. J Geotech Geoenviron Eng, ASCE 2011;137(7):704–16. https://doi.org/10.1061/(asce)gt.1943-5606.0000478.

[7] Cerato A, Victor R. Effects of long-term dynamic loading and fluctuating water table on helical anchor performance for small wind tower foundations. J Perform Constr Facil 2009;23(4):251–61. https://doi.org/10.1061/(ASCE)CF.1943-5509.0000013.

[8] Livneh B, El Naggar MH. Axial testing and numerical modeling of square shaft helical piles under compressive and tensile loading. Can Geotech J 2008;45(8):1142–55. https://doi.org/10.1139/T08-044.

[9] Rao SN, Prasad YVSN. Estimation of uplift capacity of helical anchors in clays. J Geotech Eng, ASCE 1993;119(2):352–7. https://doi.org/10.1061/(asce)0733-9410(1993)119:2(352).

[10] Ghaly A, Hanna A, Hanna M. Uplift behavior of screw anchors in sand. I: Dry sand. J Geotech Eng, ASCE 1991;117(5):773–93. https://doi.org/10.1061/(asce)0733-9410(1991)117:5(773).

[11] Li W, Deng L. Axial load tests and numerical modeling of single-helix piles in cohesive and cohesionless soils. Acta Geotech 2019;14(2):461–75. https://doi.org/10.1007/s11440-018-0669-y.

[12] Elkasabgy M, El Naggar MH. Axial compressive response of large-capacity helical and driven steel piles in cohesive soil. Can Geotech J 2015;52(2):224–43. https://doi.org/10.1139/cgj-2012-0331.

[13] Gavin K, Doherty P, Tolooiyan A. Field investigation of the axial resistance of helical piles in dense sand. Can Geotech J 2014;51(11):1343–54. https://doi.org/10.1139/cgj-2012-0463.

[14] Elkasabgy M, El Naggar MH. Dynamic response of vertically loaded helical and driven steel piles. Can Geotech J 2013;50(5):521–35. https://doi.org/10.1139/cgj-2011-0126.

[15] Elsherbiny ZH, El Naggar MH. Axial compressive capacity of helical piles from field tests and numerical study. Can Geotech J 2013;50(12):1191–203. https://doi.org/10.1139/cgj-2012-0487.

[16] El Sharnouby MM, El Naggar MH. Field investigation of axial monotonic and cyclic performance of reinforced helical pulldown micropiles. Can Geotech J 2012;49(5):560–73. https://doi.org/10.1139/t2012-017.

[17] Sakr M. Performance of helical piles in oil sand. Can Geotech J 2009;46(9):1046–61. https://doi.org/10.1139/t09-044.

[18] Guo H. Investigation on punching behavior of pile cap under column reinforced by section steel truss. ACI Struct J 2018;115(2):379–90. https://doi.org/10.14359/51700948.

[19] Tortola LM, Pallares L, Miguel PF. Punching shear failure in three-pile caps: Influence of the shear span-depth ratio and secondary reinforcement. Eng Struct 2018;155:127–43. https://doi.org/10.1016/j.engstruct.2017.10.077.

[20] Kueres D, Ricker M, Hegger J. Improved shear reinforcement for footings-punching strength inside shear-reinforced zone. ACI Struct J 2017;114(6):1445–56. https://doi.org/10.14359/51689499.

[21] Melèndez C, Miguel PF, Luis Pallarès. A simplied apporach for the ultimate limit state analysis of three-dimensional reinforced concrete elements. Eng Struct 2016;123(15):330–40. https://doi.org/10.1016/j.engstruct.2016.05.039.

[22] Zhou Y, Guoliang Dai. Parameter study of a new strut-and-tie model for a thick cap with six piles. International Journal of Geomechanics, ASCE 2016;16(1):1–11. https://doi.org/10.1061/(asce)gm.1943-5622.0000515.

[23] Hedebratt J, Silfwerbrand J. Full-scale test of a pile supported steel fibre concrete slab. Mater Struct 2014;47(4):647–66. https://doi.org/10.1617/s11527-013-0086-5.

[24] Delalibera RG, Giongo JS. Numerical analysis of two pile caps with sockets embedded, subject the eccentric compression load. Ibracon Struct Mater J 2013;6(3):436–74. https://doi.org/10.1590/S1983-41952013000300007.

[25] Xiao Y, Chen L. Behavior of model steel H-pile-to-pile-cap connections. J Constr Steel Res 2013;80:153–62. https://doi.org/10.1016/j.jcsr.2012.09.008.

[26] Bloodworth AG, Cao J, Xu M. Numerical modeling of shear behavior of reinforced concrete pile caps. J Struct Eng, ASCE 2012;138(6):708–17. https://doi.org/10.1061/(asce)st.1943-541x.0000499.

[27] Jensen UG, Hoang LC. Collapse mechanisms and strength prediction of reinforced concrete pile caps. Eng Struct 2012;35:203–14. https://doi.org/10.1016/j.engstruct.2011.11.006.

[28] Richards PW, Rollins KM, Stenlund TE. Experimental testing of pile-to-cap connections for embedded pipe piles. J Bridge Eng 2011;16(2):286–94. https://doi.org/10.1061/(ASCE)BE.1943-5592.0000144.

[29] Xiao Y, Zhang Z, Hu J, Kunnath SK. Seismic Behavior of CFT column and steel pile footings. J Bridge Eng 2011;16(5):575–86. https://doi.org/10.1061/(ASCE)BE.1943-5592.0000198.

[30] Cao J. The shear behaviour of the reinforced concrete four-pile caps. Southampton, UK: Ph.D. Thesis, School of Civil Engineering and the Environment, University of Southampton; 2009, 287 p. Retrieved from https://eprints.soton.ac.uk/73699/ [accessed 07/05/2021].

[31] Perko HA. Helical piles: A practical guide to design and installation. New Jersey: John Wiley & Sons, Inc.; 2009, p .512 [ISBN: 978-0-470-40479-9].

[32] Park J, Kuchma D, Souza R. Strength predictions of pile caps by a strut-and-tie model approach. Can J Civ Eng 2008;35(12):1399–413. https://doi.org/10.1139/L08-062.

[33] El Naggar MH, Youssef MA, Ahmed M. Monotonic and cyclic lateral behaviour of helical pile specialized connectors. Eng Struct 2007;29:2635–40. https://doi.org/10.1016/j.engstruct.2007.01.018.

[34] Youssef MA, El Naggar MH, Ahmed M. Monotonic and cyclic load behavior of helical pile connectors in the vertical direction. Can J Civ Eng 2006;33(1):10–8. https://doi.org/10.1139/l05-074.

[35] Chan TK, Poh CK. Behavior of precast reinforced concrete pile caps. Constr Build Mater 2000;14(2):73–8. https://doi.org/10.1016/S0950-0618(00)00006-4.

[36] Suzuki K, Otsuki K, Tsubata T. Influence of edge distance on failure mechanism of pile caps. Trans Japan Concr Inst 2000;22:361–7. Retrieved from https://ci.nii.ac.jp/naid/10007467724/ [accessed 07/05/2021].

[37] Otsuki K, Suzuki K. Experimental study on bending ultimate strength of four-pile caps. Trans. Japan Concr Instit 1996;482:93–102. Retrieved from https://ci.nii.ac.jp/naid/110004303171 [accessed 07/05/2021].

[38] Adebar P, Kuchma D, Collins MP. Strut-and-tie models for the design of pile caps: an experimental study. ACI Struct J 1990;87(1):81–92. Retrieved from https://trid.trb.org/view/307069 [accessed 07/05/2021].

[39] Diab MAM. Behavior of helical pile connectors for new foundations. London, Ontario, Canada: Ph.D. Thesis, School of Civil and Environment Engineering, University of Western Ontario; 2015, p. 638. Retrieved from https://ir.lib.uwo.ca/cgi/viewcontent.cgi?article=4736&context=etd [accessed 07/05/2021].

[40] Labuda T, Corley GW, Murphy M. Failure investigation of a helical anchor tie-down system supporting an olympic size swimming pool. In Proceedings of the Seventh International Conference on Case Histories in Geotechnical Engineering, Chicago, April 29–May 4, Scholoars' Mine, Missouri University of Science and Technology, 2013, p. 7. Retrieved from https://scholarsmine.mst.edu/icchge/7icchge/session08/10/ [accessed 07/05/2021].

[41] Sharma A, Guner S. System-level modeling methodology for capturing the pile cap, helical pile group, and soil interaction under uplift loads". Eng Struct 2020;220:1–14. https://doi.org/10.1016/j.engstruct.2020.110977.

[42] CRSI. Design guide for pile caps, 1st ed. Schaumburg, IL: Concrete Reinforcing Steel Institute; 2015, p. 156. Retrieved from http://resources.crsi.org/resources/design-guide-for-pile-caps/ [accessed 07/05/2021].

[43] ACI Committee 318. Building code requirements for structural concrete and commentary (ACI 318–19). Farmington Hills, MI: American Concrete Institute; 2019, p. 623.

[44] VTAG. VecTor2: Nonlinear finite element analysis software for reinforced concrete structures. VecTor Analysis Group (VTAG) Version 2.9; 2009. Retrieved from www. http://vectoranalysisgroup.com/ [accessed 07/05/2021].

[45] Vecchio FJ. Disturbed stress field model for reinforced concrete: formulation. J Struct Eng 2000;126(8):1070–7. https://doi.org/10.1061/(asce)0733-9445(2000)126:9(1070).

[46] Vecchio FJ, Collins MP. The modified compression field theory for reinforced concrete elements subject to shear. ACI J 1986;83(2):219–31. https://doi.org/10.14359/10416.

[47] CSA A23.3. Design of concrete structures. Mississauga ON: Canadian Standards Association; 2014, p. 668.

[48] AASHTO. LRFD bridge design specifications. Customary US units. 8th ed. Washington, DC: American Association of State Highway and Transportation Officials; 2017, p. 1755.

[49] Wong PS, Vecchio FJ, Trommels H. VecTor2 and formworks user's manual. ON, Canada: Technical Report, Department of Civil Engineering, University of Toronto; 2013, p. 347. Retrieved from http://www.vectoranalysisgroup.com/user_manuals/manual1.pdf [accessed 07/05/2021].

[50] Akkaya Y, Guner S, Vecchio FJ. A constitutive model for the inelastic buckling behavior of reinforcing bars. ACI Struct J 2019;116(3):195–204. Retrieved from http://www.utoledo.edu/engineering/faculty/serhan-guner/docs/JP11_Akkaya_et_al_2019.pdf [accessed 07/05/2021].

[51] Almeida Jr SA, Guner S. A practical methodology for the analysis of adhesive anchors in adverse environments for hurricane resilience. Eng Struct 2020;212:1–9. https://doi.org/10.1016/j.engstruct.2020.110505.

[52] Almeida Jr SA. Modeling of concrete anchors supporting non-structural components subjected to strong wind and adverse environmental conditions. OH, USA: MS Thesis, Department of Civil and Environmental Engineering, University of Toledo, 2015, p. 105. Retrieved from https://www.utoledo.edu/engineering/faculty/serhan-guner/docs/T6_Almeida_MS_2019.pdf [accessed 07/05/2021].

[53] Almeida Jr SA, Guner S. Equivalent cone method (ECM). OH, USA: Excel Spreadsheet. University of Toledo; 2019. Retrieved from http://www.utoledo.edu/engineering/faculty/serhan-guner/docs/5S_Equivalent_Cone_Method_ECM.xlsx [accessed 07/05/2021].

[54] Almeida Jr SA, Guner S. Equivalent cone method (ECM). OH, USA: Youtube Video, University of Toledo; 2019. Retrieved from https://www.youtube.com/watch?v=I3lpxFPtduM [accessed 07/05/2021].

[55] Chiluwal S, Guner S. Development of Design Recommendations for Helical Pile Anchorages Subjected to Cyclic Load Reversals. OH, USA: Project Report, Department of Civil and Environmental Engineering, University of Toledo, p. 170. Retrieved from http://www.utoledo.edu/engineering/faculty/serhan-guner/docs/R2_DFI_Helical_Pile_Anchorages.pdf [accessed 07/05/2021].

[56] Fisher RA. Statistical methods for research workers. In: Kotz S, Johnson NL, editors. Breakthroughs in Statistics. Springer Series in Statistics (Perspectives in Statistics). New York: Springer; 1992. p. 360.

[57] Montgomery DC. Design and analysis of experiments. 8th ed. Hoboken: John Wiley & Sons Inc; 2013. p. 724.